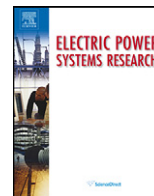




Contents lists available at SciVerse ScienceDirect

Electric Power Systems Research

journal homepage: www.elsevier.com/locate/epsr

Detection and estimation of demagnetization faults in permanent magnet synchronous motors

Subhadeep Chakraborty^a, Eric Keller^b, Asok Ray^{b,*}, Jeffrey Mayer^b

^a The University of Tennessee, Knoxville, TN 37996, USA

^b The Pennsylvania State University, University Park, PA 16802, USA

ARTICLE INFO

Article history:

Received 18 July 2011

Received in revised form

19 September 2012

Accepted 13 November 2012

Keywords:

Fault detection in PMSM

Symbolic dynamics

System identification

Fixed-structure automata

ABSTRACT

This paper presents a symbolic dynamic method for health monitoring of permanent magnet synchronous motors (PMSMs), which involves abstraction of a qualitative description from a dynamical system representation of the PMSM. The underlying algorithms rely on state-space embedding of the PMSM's output line current and discretization of the resultant pseudo-state and input spaces. System identification is achieved through inference of the PMSM's dynamical system behavior, and the deviation of the system's output behavior from the nominal expected behavior yields a measure of the estimated fault. A special-purpose test bed has been designed and fabricated for experimental validation of the health monitoring algorithm via controlled accelerated deterioration of magnetization in the PMSM. The performance of the proposed algorithm has been compared with that of a classical motor current signature analysis (MCSA) procedure as well as with a benchmark particle filter for fault detection in PMSMs.

© 2012 Elsevier B.V. All rights reserved.

1. Introduction

With the advancement in modern direct drive motor/generators, power conversion, and storage technologies, it is now possible to replace several traditional mechanical, hydraulic and pneumatic mechanisms with electrical configurations. As the complexity of industrial power systems grows, their critical infrastructure increasingly depends on the reliable operation of electrical subsystems. Consequently, it becomes imperative to develop advanced technologies for prognostics, diagnostics and health management of the power system. Among rotating machines, recent years have witnessed an increasing use of the permanent magnet synchronous motor, abbreviated as PMSM in the sequel, to provide a viable and effective alternative to other types of motors. Specifically, PMSMs have many advantages that include high speed operational capability, precise torque control, high torque to current ratio, high power to weight ratio, high efficiency, and robustness to exogenous disturbances.

As a consequence, basic research on fault detection and identification (FDI) of PMSMs has gained considerable importance over the last few decades [1]. In the course of its development, along with the use of more traditional techniques, such as residual generation using parity-space tools, dedicated observer methods and

parameter identification approaches for fault detections, there has been efforts towards development of a relatively new branch of fault-detection techniques involving data-driven machine learning and non-linear time-series analysis (NTSA) using formal languages. Several data-driven techniques such as statistical linearization [2], Kalman filtering [3], particle filtering (PF) [4,5], Markov Chain Monte Carlo (MCMC) [6], Bayesian networks [7], artificial neural networks (ANN) [8], maximum likelihood estimation (MLE) [9], wavelet-based tools [10], and genetic algorithms (GA) [11] have been reported in the literature for fault detection, diagnosis and prognosis. Very recently, Ruiz et al. [12] reported a time-frequency method specifically focused on detection and diagnosis of demagnetization faults in PMSMs operating under non-stationary speed conditions. However, in many practical cases, limited on-board computational power severely restricts the use of these complex algorithms and associated optimization techniques. Furthermore, the need for data communication over bandwidth-limited wireless sensor networks often makes dimensionality reduction and data compression a necessity.

This paper addresses the problem of detection and identification of demagnetization faults and estimation of the fault magnitude in PMSMs, without a high-fidelity component-level model of the system. Demagnetization in PMSMs may occur if induced eddy currents cause overheating in the magnets. As the magnetic properties of the rare earth magnetic materials, such as Sm–Co and Nd–Fe–Bi are highly temperature-dependent, over-heating may induce partial demagnetization of the material, resulting in reduction of available torque, torque pulsation, vibration and excessive

* Corresponding author.

E-mail addresses: schakrab@utk.edu (S. Chakraborty), eekeller@psu.edu (E. Keller), axr2@psu.edu (A. Ray), mayer@enr.psu.edu (J. Mayer).

heat. Different fault detection and diagnostic methods have been applied to detect motor faults, the most common of which are frequency domain motor current signature analysis (MCSA) and vibration analysis.

This paper reports the development of a robust non-invasive and computationally inexpensive system identification technique that is built upon formal-language-theoretic formulation, based on symbolic information. A central step in the proposed system identification method is discretization of the voltage and current time-series data for conversion into a corresponding sequence of symbols to achieve enhanced robustness and computational efficiency [13–15]. Specifically, the fault detection algorithms are designed to be robust with respect to sensor noise and, at the same time, simple enough to be implemented within the sensors themselves. This method would also facilitate construction of a reliable sensor network to serve as a backbone to the decision-making hierarchy of a system-level health and energy management system. Along with the development of the theoretical formulation, this paper also reports a novel experimental procedure for achieving controlled accelerated deterioration of magnetic strengths in PMSMs. The main contributions of this paper beyond the work reported in the authors' previous publications [13–15] are succinctly stated below.

- Formulation of a language-theoretic system identification method for fault detection under diverse steady-state operating conditions.
- Validation of the proposed fault detection, identification, and estimation algorithms on an experimental test-bed that has been designed and constructed for achieving controlled demagnetization in PMSMs.

The paper is organized in six sections. Section 2 describes the test apparatus on which the algorithms for fault detection in PMSMs have been validated. The concept and theoretical aspects of symbolic identification are presented in Section 3 along with a necessary mathematical background. The resulting fault detection scheme is developed in Section 4. The pertinent results of algorithm validation on the experimental test-bed are presented in Section 5. The paper is summarized and concluded in Section 6 along with recommendations for future research.

2. Test apparatus for fault detection in a permanent magnet synchronous motor (PMSM)

The experimental apparatus has been built and tested to validate the proposed fault diagnostic algorithms that are targeted towards detection of demagnetization failures in permanent magnet synchronous motors (PMSMs) in a realistic noisy situation. The apparatus uses the Baldor BSM50N-133AF permanent magnet synchronous motor (PMSM) that is commonly called a brushless AC servomotor; this particular series of brushless servomotor has been chosen because of its wide usage in aviation, robotics, and numerous other industrial motion control applications. The specifications of the PMSM are listed in Table 1.

Table 1
Specifications of the brushless AC servomotor.

PMSM Type	Baldor BSM50N-133AF
Rated bus voltage	160 V DC
Bus voltage used for experiments	100 V DC
Peak current	5 A
Continuous stall current	1.9 A
Rated power	190 W
Rated angular speed	4000 rpm
Torque at continuous stall current	0.45 Nm

The motor current and voltage were measured with a custom-built circuit based on Hall-effect sensors, where A/D conversion is performed by a dSpace DS1104 system that performs data acquisition and control in the apparatus. The motor drive is a custom-circuit driven by the PWM outputs of the dSpace system. The dynamometer for motor load control incorporates a Magtrol model DSP6001 controller and Hysteresis Dynamometer model HD-805-6N; however, measurements from the dynamometer were manually recorded for the experiments reported in this paper.

The next subsection presents the governing equations for the PMSM system and its electronic drive, followed by two more subsections that describe the demagnetization procedure and the experimental details, respectively.

2.1. Governing equations of the PMSM system

In state-space setting, the governing equations of the PMSM take the following form:

$$\frac{di_q^r}{dt} = \frac{v_q^r - R_s i_q^r - \omega_{re} L_d i_d^r - \omega_{re} \Lambda_{PM}}{L_q} \quad (1)$$

$$\frac{di_d^r}{dt} = \frac{v_d^r - R_s i_d^r + \omega_{re} L_q i_q^r}{L_d} \quad (2)$$

$$\frac{d\omega_r}{dt} = \frac{T_e - T_L - B\omega_r}{J} \quad (3)$$

where the subscripts q and d have their usual significance of quadrature and direct axes in the equivalent 2-phase representation, with v , i , and L being the corresponding axis voltages, stator currents and inductances. R_s is the stator resistance and $\omega_{re} = (P/2)\omega_r$ is electrical rotor velocity respectively, P being the number of pole pairs and ω_r being the rotor speed. Λ_{PM} is the flux linkage of the rotor magnets with the stator. The superscript r denotes that the equations have been set up in the rotor reference frame.

The electromagnetic torque can be expressed as:

$$T_{e,3ph} = \frac{3P}{4} \Lambda_{PM} [-i_d \sin(\theta_{re}) + i_q \cos(\theta_{re})] \quad (4)$$

where $\theta_{re} = (P/2)\theta_r$ is the electrical rotor angle. The corresponding expression for torque in the rotor reference frame is given by

$$T_{e,3ph} = \frac{3P}{4} \Lambda_{PM} i_q^r \quad (5)$$

In the above equation, the torque T_e is proportional to the quadrature axis current because the magnetic flux linkage Λ_{PM} is constant. The equation of motion is:

$$T_e = T_L + B\omega_r + J \frac{d\omega_r}{dt} \quad (6)$$

where T_L is the load torque, B is the damping coefficient, and J is the moment of inertia.

2.2. Demagnetization procedure

The electromagnetic torque in Eq. (4) is proportional to the cross-product between the current vector and the permanent magnet flux linkage vector. For a given current magnitude, the torque is maximized if the field generated by the stator windings is orthogonal to that of the permanent magnet; and the pulse width modulated (PWM) controller manipulates the three-phase line current to maintain this orthogonality.

It is noted that position feedback is vital to this scheme, since 3-phase (adc) to 2-phase (dq) conversion depends upon the rotor angle. In the present experiment, during demagnetization, an offset is added to the encoder orientation so that, instead of being orthogonal, the stator winding field opposes the field generated by

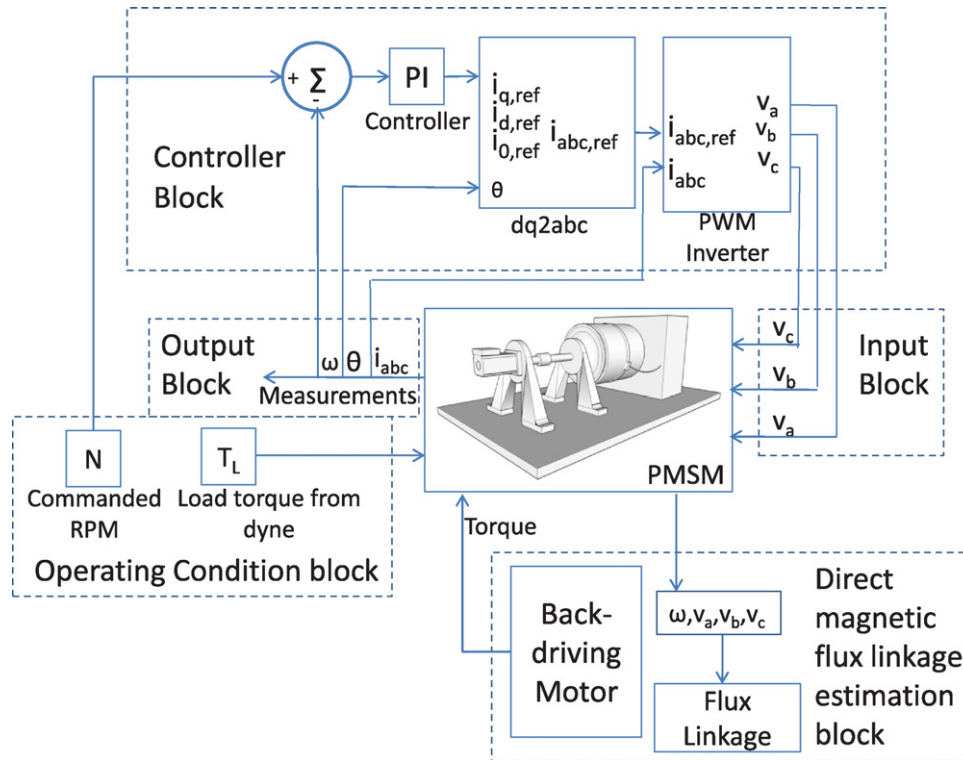


Fig. 1. Inverter-driven permanent magnet synchronous motor system.

the permanent magnets. Thus, since the two fields are anti-aligned, no torque is generated, instead the permanent magnets slowly lose their magnetism. The considerable amount of heat generated in the process enhances the loss of magnetic property in the permanent magnets. The schematic of the entire experimental apparatus is shown in Fig. 1. It is divided into several blocks, each of which is described next.

2.2.1. Controller block

The PMSM used in the experiment is a 3-phase 4-pole device rated at 160 V bus voltage, 4000 rpm; it is fed by a PWM inverter. The stator resistance of the motor is $R_s = 11.95 \Omega$; the quadrature-axis and direct-axis inductances are: $L_q = L_d = 16.5 \times 10^{-3} \text{ H}$; and the rotor inertia is $J = 0.06774 \text{ kg cm}^2$.

Two proportion-integral (PI) controllers regulate the power circuit that drives the PMSM. The inner loop regulates the stator currents, while the outer loop regulates the speed. In this control scheme, the difference between the measured speed and the reference speed generates the command quadrature axis current, which is directly proportional to the electromagnetic torque. The line currents i_a , i_b , and i_c are then measured. The reference values are compared with the actual values of the currents, and the error signal, thus constructed is used for generating the gate turn on/off commands.

2.2.2. Direct magnetic flux linkage estimation block

As the permanent magnet inside the PMSM slowly deteriorates, it is imperative to be able to measure the extent of demagnetization by some kind of direct technique so that the degree of fault predicted by the proposed syntactic method is mapped to this physical quantity.

Several researchers have estimated the flux of a PMSM and the no-load test method has become very popular in this context, where an auxiliary motor is required to drive the PMSM at a constant speed. The windings of PMSM are kept open-circuit so that the

flux can be estimated by measuring the back-EMF of the PMSM. The two-phase stator voltage $\vec{v}^r = [v_d^r \ v_q^r]^T$ in the rotor reference frame is given by

$$\vec{v}^r = R\vec{i}^r + L\frac{d}{dt}\vec{i}^r + \omega_{re}J(L\vec{i}^r + \vec{\Lambda}_{PM}^r) \quad (7)$$

where

$$\vec{i}^r = \begin{bmatrix} i_d^r \\ i_q^r \end{bmatrix}, \quad J \triangleq \begin{bmatrix} 0 & -1 \\ 1 & 0 \end{bmatrix} \quad \text{and} \quad \vec{\Lambda}_{PM}^r = \begin{bmatrix} \Lambda_{PM} \\ 0 \end{bmatrix}$$

are the current vector, 90° rotation matrix and the permanent flux linkage vector, respectively. Under steady state conditions, the derivative of the current vector is zero, and the voltage expression becomes:

$$\vec{V}^r = R\vec{I}^r + \Omega_{re}J(L\vec{I}^r + \vec{\Lambda}_{PM}^r) \quad (8)$$

where V , I and Ω_{re} are the steady state voltage, current and electrical rotor velocity. In open circuit there are no currents flowing in the windings of the machine, so the voltage is entirely due to the permanent magnet flux linkage, hence

$$\|\vec{V}\| = \|\Omega_{re}J\vec{\Lambda}_{PM}^r\| = \frac{P}{2}\Omega_r\Lambda_{PM} \quad (9)$$

The permanent magnet flux linkage is therefore

$$\Lambda_{PM} = \frac{\|\vec{V}\|}{(P/2)\Omega_r} = \frac{(\sqrt{(2/3)}V_{l-l})_{RMS}}{(P/2)((2\pi \text{ rpm})/60)} \quad (10)$$

In this experiment, at each stage of demagnetization, the line-to-line voltage and the motor speed in rpm is recorded. The permanent magnet flux linkage is estimated from these, following Eq. (10).

2.2.3. Operating condition block

The desired rpm and the load torque is set in the operating condition block. The load torque is directly set by the dynamometer.

2.2.4. Input and output block

All the variables are captured and stored in the output block, while the input voltage commands are also saved in the input block. The sensors used in the experimental apparatus are (closed-loop compensated) Hall Effect current transducers LA 55-P, procured from the manufacturer Liaisons Electroniques et Mecaniques (LEM). These current sensors are controlled by using a LM124 chip that consists of four independent, high gain, internally frequency-compensated operational amplifiers (Op-Amps). These Op-Amps are designed specifically to operate from a single power supply over a wide range of voltages. The LA 55-P sensors have a frequency bandwidth of DC to 200 kHz and an accuracy of $\pm 0.65\%$ at 50 A, 25 °C and ± 15 V power supply.

It is noted that the controller block and the direct magnetic flux linkage estimation block in Fig. 1 are never engaged simultaneously, because that would result in a conflict between the external auxiliary motor and the PMSM controller.

2.3. Details of the experimental procedure

In each set of experiments, the following order of the procedure is maintained.

- 1 A direct estimation of the magnetic flux is made and the temperature is noted.
- 2 Voltage and line current data are recorded by making the motor spin at 1000 rpm. Two sets of data are collected, corresponding to the load torques of 0.170 N m (1.5 lbf in.) and 0.226 N m (2.0 lbf in.), respectively. It is noted that the controller actively adjusts for any deterioration in the system components in the control loop.
- 3 The motor is demagnetized following the procedure outlined in Section 2.2 until the temperature rises to a predetermined value. In this experiment, the rise in temperature of the motor, which is an effect of this demagnetization procedure, is also used as an indicator of how much the demagnetization has progressed.
- 4 The procedure is repeated from Step 1.

The whole experiment has been repeated 14 times to assess the robustness of the procedure. At the end of each individual demagnetization run and the corresponding reduction in the magnetic flux linkage is measured by the no-load test method described in Section 2.2.2. Fig. 2 presents the profile of percent reduction in magnetic flux as a function of the core temperature.

It is noted that the temperature of the permanent magnet serves only as a qualitative guide to the experimenters to indicate that the motor has demagnetized to a certain predetermined value. The unique one-to-one correspondence between the temperature and magnetic flux linkage was experimentally verified and the result has been presented in Fig. 2. Apart from being used as this preliminary guide, temperature has not been subsequently used for determining the receiver operating characteristics (ROC) (see Section 5). Direct tests, described in Section 2.2.2, have been performed for that purpose, and these results have been used for validating the predictions obtained by symbolic identification.

3. Concept of symbolic identification

Since sufficiently accurate and robust continuous-domain models of physical processes may not be always available, it is logical to construct a semantic model of such processes to capture their pertinent behavior. In this context, estimation of deviations of such a system's behavior from its nominal behavior can be realized in the abstract symbolic domain with grammatical inference techniques. Specifically for PMSMs, time-series data (that consist of voltage and

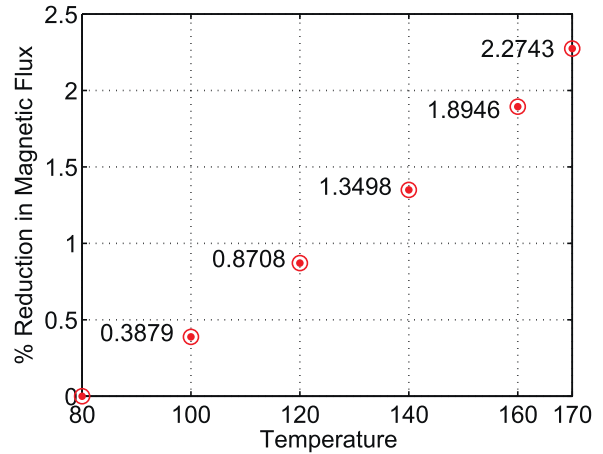


Fig. 2. Variation of magnetic flux linkage with temperature.

current signals recorded by a data-acquisition system) could be discretized temporally and spatially to generate symbol strings as representatives of their behavior. The underlying theory of symbol generation, adopted in this paper, is based on the previous work of the authors, which has been reported in recent literature [13,14,16]. The core concept here is built upon the fundamental principles of symbolic dynamics, finite state automata, and pattern recognition and is succinctly described below. Fig. 3 illustrates the concept of partitioning.

A block of data (e.g., time series) is converted to a symbol string by partitioning into finitely many discrete cells, $\Phi_1, \Phi_2, \dots, \Phi_m$. These cells form an exhaustive and mutually exclusive set, i.e.,

$$\bigcup_{j=1}^{|\Sigma|} \Phi_j = \Omega \quad \text{and} \quad \Phi_j \cap \Phi_k = \emptyset \quad \forall j \neq k$$

where each cell is labeled as a symbol $\sigma \in \Sigma$. The resulting symbol set Σ is called the alphabet Σ , consisting of different symbols such that the alphabet's cardinality is $|\Sigma|$. If a data point falls in a particular partitioning cell, then it is assigned the corresponding symbol of that cell; thus, the data set is transformed into a symbol string in this manner.

In the context of symbolization, the underlying structure of a dynamical system, (in this case, the pertinent dynamics of PMSM) is captured by a quantized representation of a continuous-time continuous-state generalized dynamical system (GDS).

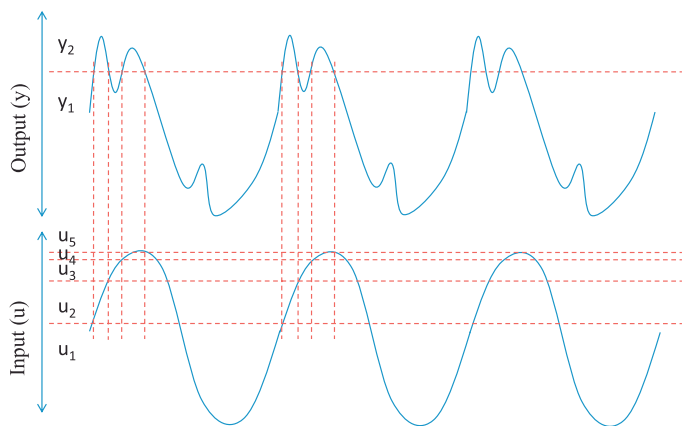


Fig. 3. Partitioning scheme for input and output data.

Definition. (Generalized dynamical system [17]) A generalized dynamical system (GDS) is defined as an 8-tuple automaton.

$$\mathcal{D} = (T, U, W, Q, P, f, g, \leq)$$

where

- T is the time set (e.g., $T = [0, \infty)$),
- U is the input set,
- W is the output set,
- Q is the set of internal states,
- \leq is an order relation on T , expressed as: $\leq \subseteq T \times T$,
- f is the global state transition function defined as

$$f : T \times T \times Q \times U \rightarrow Q \quad \text{for time-varying systems}$$

$$f : T \times Q \times U \rightarrow Q \quad \text{for time-invariant systems}$$

- g is the output function defined as

$$g : T \times Q \rightarrow W \quad \text{for time-varying systems}$$

$$g : Q \rightarrow W \quad \text{for time-invariant systems}$$

Definition. (Qualitative dynamical system) The quantized abstraction of a GDS is called a qualitative dynamical system (QDS) that is represented as a 5-tuple

$$\mathcal{G} = \{Q, \Lambda, \Sigma, \delta, \gamma\}$$

where

- $Q \triangleq \{q_1, q_2, \dots, q_f\}$ is the finite set of qualitative states of the automaton.
- $\Lambda \triangleq \{\lambda_1, \lambda_2, \dots, \lambda_m\}$ is the set of qualitative input events, called the input alphabet.
- $\Sigma \triangleq \{\sigma_1, \sigma_2, \dots, \sigma_n\}$ is the set of output symbols, called the output alphabet, where the output symbols bear a one-to-one correspondence with the quantized values of the dynamical system's outputs.
- $\delta : Q \times \Lambda \rightarrow \mathcal{F}_Q$ is the state transition function that maps the current state into the next state upon receiving the input λ . If the state transition function is probabilistic, then

$$\delta : Q \times \Lambda \rightarrow \mathcal{F}_Q$$

where \mathcal{F}_Q is the probability distribution function of the qualitative states Q .

- $\gamma : Q \rightarrow \Sigma$ is the output generation function that determines the output symbol from the current state. In its full generality, γ can be probabilistic as well, i.e.,

$$\gamma : \mathcal{F}_Q \rightarrow \mathcal{F}_\Sigma$$

where \mathcal{F}_Σ is the probability distribution function of the output alphabet Σ .

Definition. (Qualitative abstraction) A QDS \mathcal{G} is derived from a GDS \mathcal{D} via a vector function, $\chi : \mathcal{D} \rightarrow \mathcal{G}$ where $\chi \equiv (\chi_{TQU}, \chi_Q, \chi_W)$ is a 3-tuple vector function consisting of three individual abstraction functions: defined as

$$\chi_{TQU} : T \times Q \times U \rightarrow \Lambda$$

$$\chi_Q : Q \rightarrow Q$$

$$\chi_W : W \rightarrow \Sigma$$

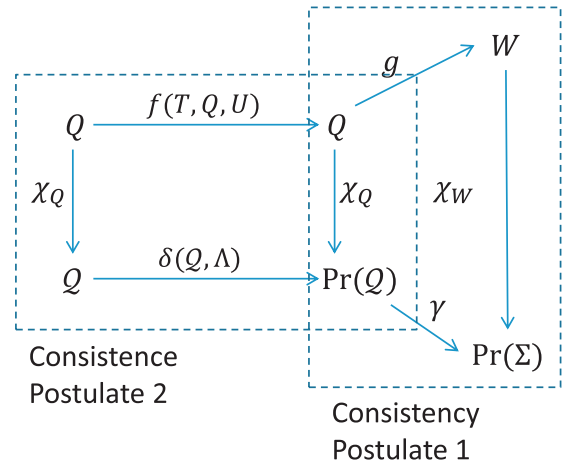


Fig. 4. Graphical representation of the consistency postulates.

In the above context, Kokar [17] introduced a set of necessary and sufficient conditions as “consistency postulates” that the pair (\mathcal{G}, χ) must satisfy in order to be a valid representation of the general dynamical system. In this paper, since the transition function δ of the QDS is probabilistic, the consistency postulates have been redefined in a probabilistic sense. The modified consistency postulates are stated as follows.

Definition. (Consistency postulates) Let \mathcal{D} , \mathcal{G} and χ represent a GDS, QDS and an abstraction function respectively. Then the pair (\mathcal{G}, χ) represents the consistency postulates in a probabilistic sense if, $\forall t \in T, q \in Q, u \in U$,

$$\text{Consistency postulate \#01: } \chi_Q(f(t, q, u)) \sim \delta(\chi_Q(q), \chi_{TQU}(t, q, u)) \quad (11)$$

$$\text{Consistency postulate \#02: } \gamma(\chi_Q(q)) = \chi_W(g(q)) \quad (12)$$

where the notation $(X \sim P)$ implies that the random variable X is distributed according to the probability distribution P .

Postulate #01 essentially restates the conditions of homomorphism, which means that partitioning followed by transition in the discrete domain is the same as transition in the continuous domain followed by partitioning, in a probabilistic sense. Postulate #02 requires that partitioning the output function is equivalent to applying the output function to the partition function. Fig. 4 along with the governing equations for GDS and QDS, introduced earlier, illustrates the concept and the following theorem presents a formal statement.

Theorem 3.1 (Kokar [17]). Let $W_\pi \equiv (W_1, \dots, W_n)$ be a finite partition of a GDS's output space W , which is given by $\chi_W^{-1} : \Sigma \rightarrow W_\pi$. Let Q_π be a partition of Q defined as an inverse image of W_π under g , i.e.,

$$Q_\pi = g^{-1}(W_\pi),$$

and let TQU_π be a partition of $T \times Q \times U$ defined as an inverse image of Q_π under f ,

$$TQU_\pi = f^{-1}Q_\pi.$$

Then, Q_π is a maximal admissible partition of Q , and TQU_π is an admissible partition of $T \times Q \times U$.

Theorem 3.1 is interpreted as follows:

- A critical hypersurface partition in Q is an image of the partition in W under g^{-1} .

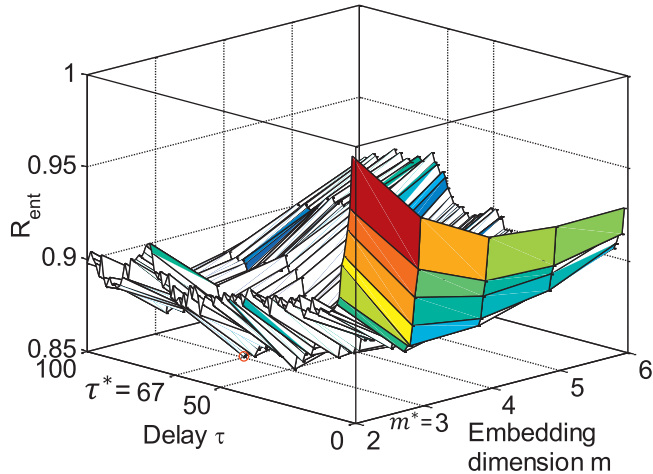


Fig. 5. Relative entropy variation with embedding dimension and delay.

- A critical hypersurface partition in $T \times Q \times U$ is an image of the partition in Q under f^{-1} .

If the system model (i.e., the functions f and g governing the GDS) is known, then the critical hypersurfaces or partitions can be analytically evaluated and utilized as delineated above. However, in the absence of model equations, the following steps are used.

- 1 There should be an alternate way of constructing the phase space from the output only without the model equations.
- 2 There should be an alternate way of arriving at the proposed partition without the information about the state transition function f and the output function g .

Next we delineate a method for construction of GDS and QDS.

Phase space construction: In the absence of a state-space model, starting from the output signal captured by suitable instrumentation, a pseudo phase-space is constructed from the delay vectors using Taken's theorem [18]. The embedded phase-space is denoted by

$$\mathbf{x}(k) = [x_{k-\tau}, \dots, x_{k-m\tau}],$$

where τ is the time lag, and m is the embedding dimension. Takens' theorem [18] guarantees that, in the noise-free case, a system of state dimension n can be embedded by using a maximum of m_T lags where $m_T \leq 2n + 1$.

Many optimization routines have been reported in literature to find optimum values of the embedding parameters m , n and τ . In this paper, the Kozachenko–Leonenko (KL) [19] estimate of the differential entropy R_{ent} (e.g., obtained from the output current signal i_c of the PMSM) is minimized to find the optimal set of embedding parameters (m^* , τ^*). Fig. 5 shows the variation of R_{ent} with increasing m and τ , where the infimum occurs at $m^* = 3$ and $\tau^* = 67$ for the PMSM system.

In the very next step, the phase space and the input space are individually discretized. The crux of the method is to place the partitions in such a way, that there is a change in both input and output alphabets at exactly the same instant.

Partitioning: Time series sensor data are obtained from the input and output data streams of the dynamical system \mathcal{D}_0 under nominal condition under different input conditions. Let $\mathcal{Y} = \{y_1, y_2, \dots\}$, $y_k \in \Sigma$ denote the discretized output sequence. The next step is to construct a probabilistic finite state automaton (PFSA). In this paper, a D -Markov machine is next constructed, with states defined by symbol blocks of length D from \mathcal{Y} . The reader is

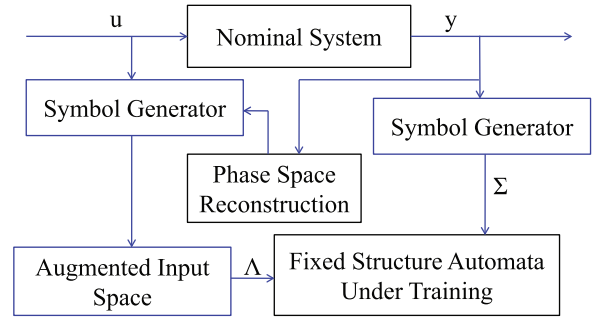


Fig. 6. Learning scheme for system identification.

referred to Refs. [13] and [14] for an in-depth description of the procedure.

3.1. Identification and learning

A partition constructed in this way is admissible [20], but may not be maximal, since this partition is a subpartition of the original partition proposed in Theorem 3.1. Next we present a learning scheme, depicted in Fig. 6, that explains identification of the state transition function δ from the input–output symbol sequences obtained from experiment on the system while it is under nominal condition.

It is assumed that inputs and outputs are time-synchronized. The state transition function δ can be expanded into two dimensional matrices δ^{λ_i} , indexed by the input variable alphabets. That means

$$\delta = \{\delta^{\lambda_1}, \delta^{\lambda_2}, \dots, \delta^{\lambda_m}\} \quad (13)$$

where $\delta^{\lambda_i} : q_j \times \lambda_i \rightarrow Pr\{Q\}$ maps the current state q_j and input λ_i to the probability distribution over all possible states in the set Q . The algorithm for estimating the matrices δ^{λ_i} is straightforward and involves counting the frequency of each transition in the learning phase. Since the state transition matrices are constructed simply by counting, this method is well-suited for implementing in the sensor electronics for real-time prognoses.

The learning algorithm has to make sure that the probability values of δ^i converge. In this context, convergence of the probability values require that the sensor time-series data collected should be statistically stationary [13]. This can be ensured if the data collection for FDI analysis is scheduled during only steady state operation of the motor. The convergence depends on the length of the input–output symbol sequences. In this work, a stopping rule [16] has been used for detecting the optimal data length. In the learning phase, it has to be ensured that the grammar \mathcal{G} is trained with sufficient input data belonging to a particular equivalence class. This is the so-called *coverage problem*.

4. Fault detection scheme

The concept of fault detection is largely similar to that of the learning scheme in Fig. 6 with the following exception. The input and output time series data from the actual plant are discretized to form symbol sequences, which are fed to the trained fixed-structure automaton. The discretization is performed using the same partitioning as was done during the learning phase. It is noted that the resulting finite state automaton (FSA) uses the output from the actual system in addition to the input, and hence cannot serve as an independent ‘system identification’ procedure in the classical sense of the term. Nevertheless the automaton can serve as a system emulator if the state transition function δ is completely

deterministic. That is, given the current state q_j and the current input symbol λ_i ,

$$\delta^{\lambda_i}(q_j, \lambda_i) = [p_{q_1} \ p_{q_2} \ \dots \ p_{q_{|\Sigma|}}]^T \quad (14)$$

$$\text{where } p_{q_k} = 1 \text{ for one and only one } k \quad (15)$$

$$= 0 \text{ otherwise} \quad (16)$$

By redefining the partitioning and depth used for the construction of states, a stochastic automaton can be converted to a deterministic finite state automata [21]. But that transformation inevitably leads to state explosion and uneconomical growth in the computational complexity.

Instead, in the current scheme, the state transition probability vectors $\pi_{q_j}^{\lambda_i}$, which are the rows of the state transition matrix δ , serve as feature vectors, and are used for the purpose of fault detection. An extremely convenient feature of using state transition probabilities as feature vectors, and using stochastic methods to define distances between nominal and off-nominal behavior of plants is that this technique is very robust to noise.

This paper proposes a *pseudo-learning* technique of utilizing the stochastic state transition function δ for the purpose of fault detection. In this method, the actual state transitions inside the fixed-structure automaton in the fault detection phase occur according to the output symbol sequence obtained from the actual system; and, at each instant of state transition, the trained automaton produces a *state transition probability vector* π_n [21] that represents the characteristics of the nominal system corresponding to inputs at this n th instant.

It is noted that the pattern vector π_n , produced by the trained automaton, is characteristic of the nominal behavior of the plant given the past history of input, state and output. The current (possibly off-nominal) condition of the plant is characterized by another state probability vector $\tilde{\pi}_n$. This is defined for the actual system output at an instant n , for which only one element of the vector will be 1, rest are zeros. The next step is to use the sequences of instantaneous State Probability vectors $\{\pi_n\}$ and $\{\tilde{\pi}_n\}$ obtained at each time instant, to construct a pattern vector. Under the assumption of ergodicity of the system, a pattern can be generated from frequency count of the state visits over a wide time window in case of symbolic time series analysis [13]. The equivalent process in the present case would be calculation of mean State Probability vectors \mathbf{p} and $\tilde{\mathbf{p}}$ from the collections $\{\pi_1, \pi_2, \dots, \pi_n\}$ and $\{\tilde{\pi}_1, \tilde{\pi}_2, \dots, \tilde{\pi}_n\}$ respectively over time instants 1, 2, ..., n . It may be noted that in an ideal case, \mathbf{p} should converge to $\tilde{\mathbf{p}}$, while they should start to diverge from each other as the fault progresses. Thus any measure of divergence of the two probability vectors, such as the difference, $\mathbf{p} - \tilde{\mathbf{p}}$ is a natural choice for constructing the pattern vector corresponding to that specific fault condition. Once the pattern vectors for a fault condition are obtained, a suitable classification algorithm, such as a support vector machine [22] can be utilized to create the hyperplane separating the nominal patterns from the possibly off-nominal pattern vectors.

Remark. In the *Learning Automata* literature, *learning* [21] is done by continuous feedback from environment to the automaton at each time instant. Here also similar feedback technique is taken but not for learning or changing the structure or internal functions of the finite state machine, but only to provide actual history of past outputs to the nominal automaton based model. Thus the technique is called *pseudo learning*.

5. Results and discussion

This section presents the results of experimental validation of the symbolic identification algorithm for fault detection in PMSMs. The training set is comprised of the input signal profile of one of

the three line voltages (v_c) and the output signal profile of the line current (i_c) for different load conditions. Fault detection and identification (FDI) techniques using the stator current vector in the rotor (Park's) reference frame have been widely reported in literature in the past. However, in this paper, only i_c and v_c have been utilized in order to validate the effectiveness of the analysis technique with only partially available sensor data. Moreover, directly using sensor data leads to simpler hardware and software design.

The data from different load conditions are concatenated to form the complete output set. The resulting time series is then discretized by using the maximum entropy partitioning (MEP) [14] to construct probabilistic finite state automata (PFSA) [13] for three different values, 5, 15, and 25, of the alphabet size $|\Sigma|$. The objective here is to evaluate the impact of the alphabet size $|\Sigma|$ (and hence the number of PFSA states) on the performance of the detection algorithm. Following the procedure outlined in Section 3.1, the embedding dimension and time lag are chosen to be $m^* = 3$ and $\tau^* = 67$, respectively. The variation of relative entropy with the delay and embedding dimension is plotted in Fig. 5. The augmented input space is then constructed by discretizing the input and phase space. The input specific probabilistic state transition matrices are next constructed, which concludes the training of the PFSA.

In the validation part, the input and output data corresponding to a single fault level (e.g., a loss of 0.39% of PMSM magnetic strength) are fed into the algorithm for different load conditions. The pattern vector cluster, formed by the data from multiple runs and different load conditions, corresponding to this fault condition is calculated according to the algorithm described in Section 4. The data set in its entirety consists of 14 experiments, where each experiment consists of two load conditions and six (de)magnetization levels. In other words, each (de)magnetization level is characterized by 28 data sets, and consequently 28 pattern vectors. As an example, for distinction between the nominal and 0.39% demagnetized level (say), there are $28 \times 2 = 56$ pattern vectors out of which 28 belong to the nominal class and the remaining 28 belong to the 0.39% demagnetized class. The success or failure of the algorithm depends on how these patterns can be distinguished from the pattern cluster generated by the machine when the motor was running in its nominal health state, albeit at different load conditions.

A support vector machine (SVM) with linear kernel [22] has been used to classify the nominal condition from the off-nominal conditions. For plotting the receiver operating characteristic (ROC) curves for each fault condition, 55 out of the 56 patterns were used as training data, and the remaining 1 as the test data. This process was then repeated 56 times, each time choosing a different pattern vector as the test case. This procedure, called 'leave-one-out-cross-validation' [22], yielded 56 instances of the test case being correctly or incorrectly classified. From this information, the true positive rate (TPR), true negative rate (TNR), false positive rate (FPR) and false negative rate (FNR) were calculated, where "positive" denotes nominal behavior and "negative" denotes off-nominal behavior. Thus, a false positive implies a missed event, i.e., a faulty motor is classified as healthy, and a false negative implies a false alarm, i.e., a healthy motor is misclassified as faulty.

The SVM classifier is trained with both nominal and faulty data. This process necessitates collection of faulty data by demagnetizing a machine and then using this data-bank to tune the SVM classifier to be subsequently used for similar machines. In order to assess the effectiveness of the fault detection technique in different machines, data generated by a model has been used for training, which will make the approach 'machine-invariant'. However, the usefulness of this approach could be limited due to intrinsic inadequacies of the lumped parameter models to generate representative data as well as due to the limitations of obtaining the machine parameters. As an alternative, one may adopt external validation, where

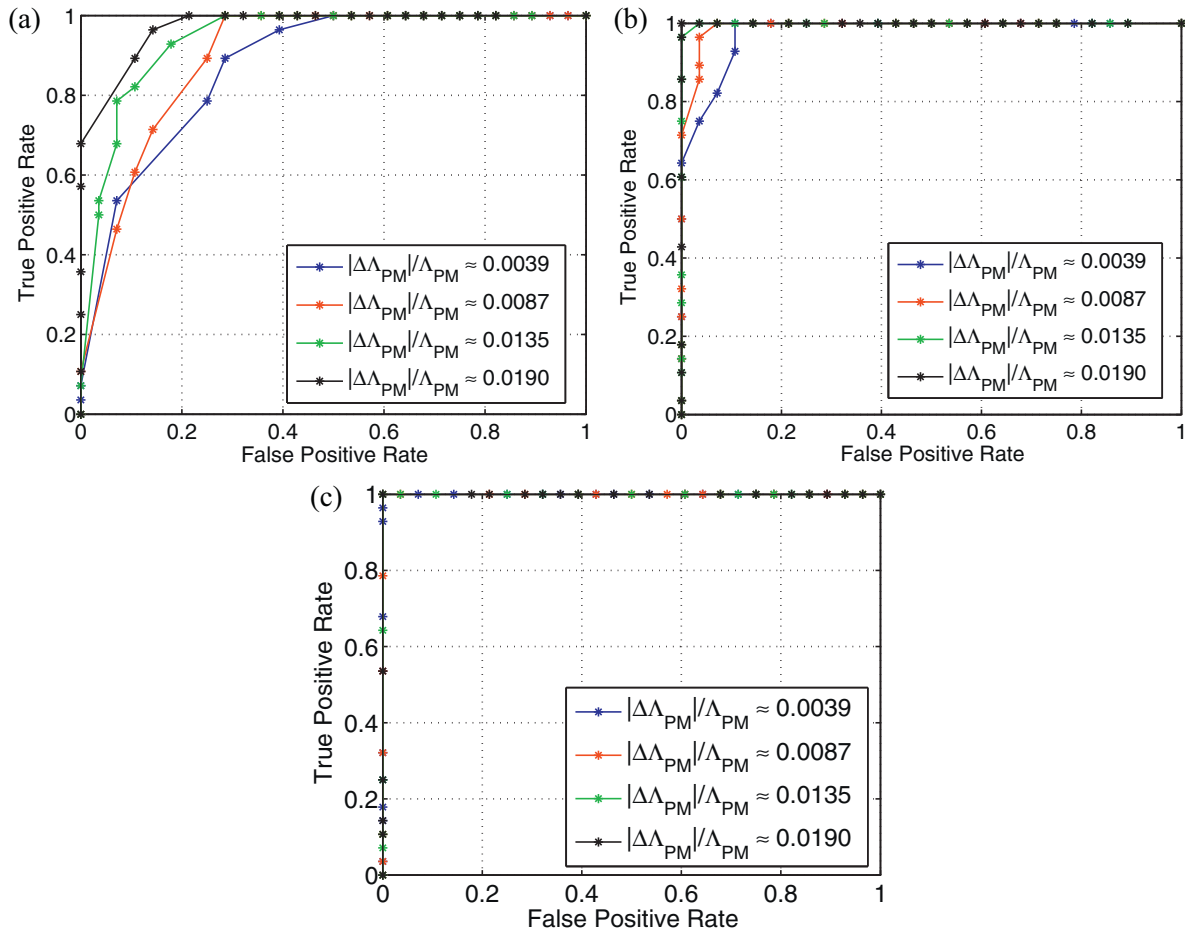


Fig. 7. Receiver operating characteristics (ROC) of symbolic identification and support vector classification for different alphabet size $|\Sigma|$.

the data generated from one machine are used for training and the data generated from other machines are used for testing. This approach is expected to yield a more accurate estimate of the effectiveness of the underlying algorithm. This issue is a topic of future research.

The three plates in Fig. 7 show three families of receiver operating characteristic (ROC) plots of the SVM classifier when applied to pattern vectors corresponding to different motor health conditions. The left hand plot in Fig. 7(a) shows that, for $|\Sigma| = 5$, the ROC curves move away from the top left hand corner implying that this alphabet size lacks the resolving capacity to distinguish between nominal signal and weak fault signatures. Only for larger levels of fault, does the ROC move closer to the left hand top corner. In Fig. 7(b), where $|\Sigma|$ is increased to 15, the family of ROC plots moves toward the top left hand corner, which shows that both detection and false alarm rates improve although the trend remains similar; this shows that it is possible to choose a $|\Sigma|_{min}$ below which the classifier performance becomes unacceptable. In Fig. 7(c), where $|\Sigma|$ is further increased to 25, it is seen that even a deviation as small as 0.39% is correctly detected at different levels of demagnetization, where $TPR \rightarrow 100\%$ and $FPR \rightarrow 0\%$. Thus, both TPR and FPR improve as the alphabet size $|\Sigma|$ is increased up to a certain level. A possible reason for this performance enhancement is that an increase in $|\Sigma|$ is equivalent to reduced effects of quantization due to finer partitioning of the time series. However, this performance gain is achieved at a higher computational cost (i.e., increased execution time and memory requirements). Optimal selection of $|\Sigma|$ by trade-off between detection performance and computation cost is a topic of future research.

Table 2
Computational cost for different alphabet size $|\Sigma|$.

Computational cost	Alphabet size		
	5	15	25
Execution time (s)	57.65	110.80	1137.73
Memory required (MB)	142	157	295

Table 2 presents a comparative evaluation of the computational cost (i.e., execution time and memory requirements) of the algorithm different alphabet size $|\Sigma|$. These results were obtained by executing the MATLAB R2011a codes on a Dell Inspiron Workstation with 8GB of RAM and an Intel Xeon dual processor CPU.

Tables 3–5 list the data for TPR and FPR to represent the families of ROC plots in the three plates of Fig. 7 for $|\Sigma| = 5, 15$ and 25, respectively. For each demagnetization level, only the significant data points have been reported. For example, in Table 5, since the curves for $|\Sigma| = 25$ are perfect straight lines indicating ~100% detection rate, only three points, namely $TPR/FPR = 0/0, 1/0$ and $1/1$ are reported to represent the ROC data, omitting the points in between.

5.1. Comparison with motor current signature analysis (MCSA)

The previous section shows that fault detection procedure based on symbolic identification performs with nearly 100% accuracy, where incipient faults with subtle fault signatures are detected on an experimental apparatus in the presence of process and observation noise. Nevertheless, it is important to compare the proposed method of fault detection with an established procedure. One such

Table 3

Receiver operating characteristic data showing true positive rates (TPR) and false positive rates (FPR) for different levels of demagnetization using alphabet size $|\Sigma| = 5$.

Threshold level	$\frac{\Delta \Lambda_{PM}}{\Lambda_{PM}} = 0.39\%$		$\frac{\Delta \Lambda_{PM}}{\Lambda_{PM}} = 0.87\%$		$\frac{\Delta \Lambda_{PM}}{\Lambda_{PM}} = 1.35\%$		$\frac{\Delta \Lambda_{PM}}{\Lambda_{PM}} = 1.90\%$	
	TPR	FPR	TPR	FPR	TPR	FPR	TPR	FPR
1	1.0000	1.0000	1.0000	1.0000	1.0000	1.0000	1.0000	1.0000
2	1.0000	0.5000	1.0000	0.2857	1.0000	0.2857	1.0000	0.2143
3	0.9643	0.3929	0.8929	0.2500	0.9286	0.1786	0.9643	0.1429
4	0.8929	0.2857	0.7143	0.1429	0.8214	0.1071	0.8929	0.1071
5	0.7857	0.2500	0.6071	0.1071	0.7857	0.0714	0.7500	0.0714
6	0.5357	0.0714	0.4643	0.0714	0.6786	0.0714	0.6786	0
7	0.0714	0	0.1071	0	0.5357	0.0357	0	0
8	0	0	0	0	0.5000	0.0357	-	-
9	-	-	-	-	0.0714	0	-	-
10	-	-	-	-	0	0	-	-

Table 4

Receiver operating characteristic data showing true positive rates (TPR) and false positive rates (FPR) for different levels of demagnetization using alphabet size $|\Sigma| = 15$.

Threshold level	$\frac{\Delta \Lambda_{PM}}{\Lambda_{PM}} = 0.39\%$		$\frac{\Delta \Lambda_{PM}}{\Lambda_{PM}} = 0.87\%$		$\frac{\Delta \Lambda_{PM}}{\Lambda_{PM}} = 1.35\%$		$\frac{\Delta \Lambda_{PM}}{\Lambda_{PM}} = 1.90\%$	
	TPR	FPR	TPR	FPR	TPR	FPR	TPR	FPR
1	1.0000	1.0000	1.0000	1.0000	1.0000	1.0000	1.0000	1.0000
2	1.0000	0.1071	1.0000	0.0714	1.0000	0.0357	1.0000	0
3	0.9286	0.1071	0.9643	0.0357	0.9643	0	0	0
4	0.8214	0.0714	0.8929	0.0357	0	0	-	-
5	0.7500	0.0357	0.8571	0.0357	-	-	-	-
6	0.6429	0	0.0714	0	-	-	-	-
7	0	0	-	-	-	-	-	-

Table 5

Receiver operating characteristic data showing true positive rates (TPR) and false positive rates (FPR) for different levels of demagnetization using alphabet size $|\Sigma| = 25$.

Threshold level	$\frac{\Delta \Lambda_{PM}}{\Lambda_{PM}} = 0.39\%$		$\frac{\Delta \Lambda_{PM}}{\Lambda_{PM}} = 0.87\%$		$\frac{\Delta \Lambda_{PM}}{\Lambda_{PM}} = 1.35\%$		$\frac{\Delta \Lambda_{PM}}{\Lambda_{PM}} = 1.90\%$	
	TPR	FPR	TPR	FPR	TPR	FPR	TPR	FPR
1	1.0000	1.0000	1.0000	1.0000	1.0000	1.0000	1.0000	1.0000
2	1.0000	0	1.0000	0	1.0000	0	1.0000	0
3	0	0	0	0	0	0	0	0

procedure is based on motor current signature analysis (MCSA), which is widely used for detecting broken rotor bars [23] and stator winding faults [23] especially in 3-phase induction motors, and has also been used for PMSM fault detection [1]. The MCSA-based fault detection procedure is non-invasive and needs only the line currents of the motor, where the computation merely involves the fast Fourier transform (FFT) of the time series data. The execution of the FFT algorithms on a PMSM with a faulty rotor gives rise to different harmonics [1,24], which can be identified as

$$f_f = f_e \left(1 \pm \frac{k}{P} \right) \quad (17)$$

where f_f is the fault frequency, f_e is the electrical fundamental frequency, k is a positive integer, and P is the number of pole pairs. It has been shown by Roux et al. [1] that these integer multiples of the rotor frequency are the best frequency components to monitor when detecting rotor faults. The lowest fault frequency is the stator synchronous frequency divided by the number of pole pairs. In the case of the four-pole machine used in this study, the lowest fault frequency is $f_{f,min} = f_e/2 \approx 16.67$ Hz corresponding to a rotor speed of 1000rpm = 16.67 Hz, and an electrical frequency of $f_e = P/2 * \text{rotor speed} = 33.33$ Hz. Fig. 8 shows the stator current spectrum of the demagnetized motor and its comparison with that of a normal motor over the pertinent range of frequencies. However, the spectra of the faulty motor and the normal motor appeared to be essentially identical, i.e., no component could be unambiguously identified as an artifact of the demagnetization process.

Most of the motor faults investigated and reported in literature involve disruption(s) induced into the axisymmetric structure of the motor. Examples include a broken rotor bar [23,25] and

static or dynamic eccentricities [1], where the disruption of the symmetry results in the creation of new frequency peaks in the current spectrum. To address the problem of detecting unknown and unstructured faults at an early stage, the demagnetization process has been used in this paper to generate uniform weakening of the magnetic field, which represents an incipient fault of no specific nature. In this case, it is not a straight-forward task to visually

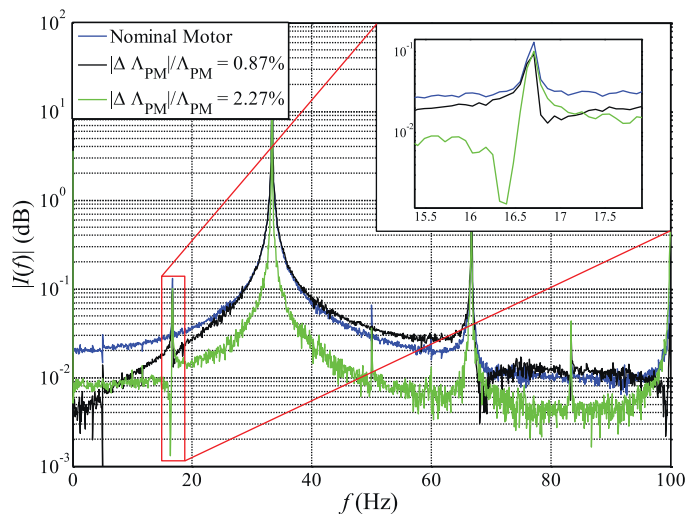


Fig. 8. Stator current spectrum (FFT) for a constant rotor speed of 1000 rpm operating at a load torque of 0.226 Nm. Inset: Current spectrum details at the fault frequency.

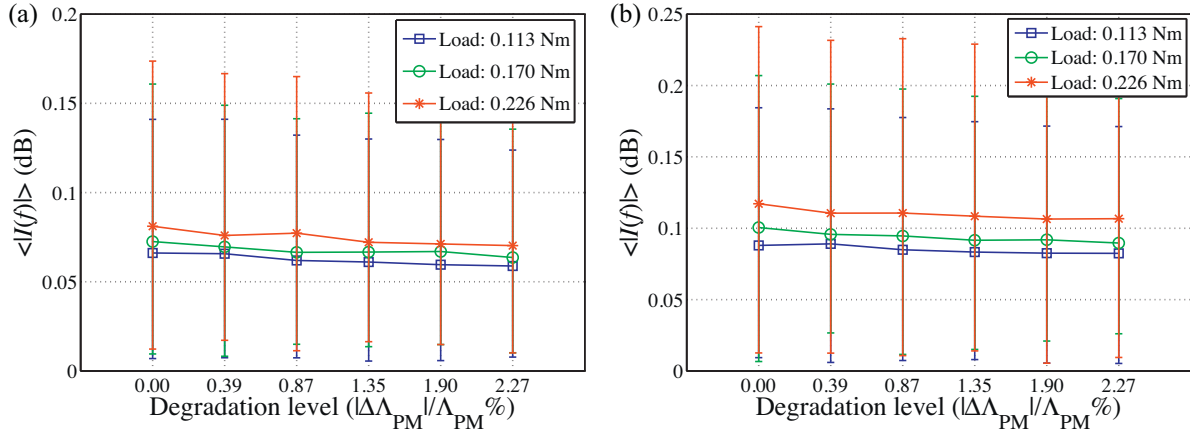


Fig. 9. Average (computed over all experiments) signal strength at (a) the fault frequency (16.67 Hz) and (b) the odd harmonics (16.67 Hz, 50 Hz and 83.35 Hz) of the lowest fault frequency as a function of degradation.

distinguish the effects of demagnetization from the current spectra. Furthermore, the lack of signature in the current spectrum is due to the low levels of demagnetization under consideration. A more severe demagnetization will no doubt have a much more noticeable effect and can be possibly detected by mere inspection of the line currents.

In order to quantify the change in the frequency content around the lowest fault frequency $f_{f,min} \approx 16.67$ Hz, the signal strength is computed around the fault frequency. Fig. 9(a) shows a clear trend in the average signal strength, computed over all the runs of the experiment and plotted against the demagnetization levels for the individual load conditions. Further analysis of the cumulative frequency contents around the fault (see Eq. (17)) shows a similar trend, as seen in Fig. 9(b). However, it appears from the close proximity of the profiles at different load conditions and small slopes of the individual plots in Fig. 9(a) and (b) that the MCSA procedure would lead to high probabilities of false alarms and missed events. In other words, MCSA may not be able to yield acceptable detection performance under modest levels of demagnetization and other unstructured faults.

5.2. Comparison with a dedicated observer method

Since the widely used MCSA technique failed to provide a robust criterion for classifying healthy from faulty motors, an observer-based technique, namely, the particle filter [26] is next chosen to serve as a benchmark fault detection algorithm.

A review of the PMSM model equations reveals the presence of two nonlinearities $\omega_{re}i_d^r$ and $\omega_{re}i_q^r$ in the first two state equations. Consequently, either particle filter or an extended/unscented version of the Kalman filter [5] become an obvious choice. The reason behind the choice of the particle filter is that, this filter works under general assumptions of non-Gaussian noise structures and non-linearities in process dynamic models.

The main features used for fault detection and the underlying algorithm are presented next for completeness of the paper.

5.3. Fault detection with particle filtering

Particle filtering involves generating a number of particles according to an initial distribution, and then passing these particles through an initial model of the system. After the first observation, the particles are weighted according to their Euclidean distance from the true observation. Sequential importance sampling (SIS) and sampling importance resampling (SIR) filters differ in the stage where the particles are resampled. In SIR filtering, the particles are

redistributed with particles of greater weight being given higher probabilities. In SIS filtering, the distribution is allowed to evolve without the effect of these weights. The histogram of these particles represents a multi-point approximation of the density function of the physical process evolving with time, and the mean and confidence intervals for the state estimates are determined from this distribution. The particle filter algorithm is presented below.

Algorithm 1. Particle Filter

- 1: Initialization: Initialize time at $k=0$ and sample N particles $\{x_k^i\}_{i=1}^N$ from an initial distribution which is assumed to be Gaussian.
- 2: **while** $k \leq k_{final}$ **do**
- 3: **for** $i = 1 : N$ **do**
- 4: Draw $x_k^i \sim q(x_k | x_{k-1}^i, y_k)$
- 5: Evaluate the importance weights up to a normalizing constant $\tilde{w}_k^i \propto w_{k-1}^i \frac{p(y_k | x_k^i) p(x_k^i | x_{k-1}^i)}{q(x_k^i | x_{k-1}^i, y_k)}$
- 6: **end for**
- 7: **for** $i = 1 : N$ **do**
- 8: Normalize $w_k^i = \frac{\tilde{w}_k^i}{\sum_{j=1}^N \tilde{w}_k^j}$
- 9: **end for**
- 10: **if** $\hat{N}_{eff} = \frac{1}{\sum_{i=1}^N (w_k^i)^2} < N_{thresh}$ **then**
- 11: Resample
- 12: **end if**
- 13: **end while**

Knowledge of the posterior density $p(x_k | \mathbf{Y}_k)$ enables calculation of the state estimate \hat{x}_k for minimum mean-squared error (MMSE), where the estimation errors are used for fault detection in the system. The basic principle is that Bayesian techniques track the system states more effectively when the system is closer to a nominal condition, and the error would be greater when the system is in an anomalous condition.

The filter is calibrated at the nominal condition of the permanent magnet flux linkage $\Lambda_{PM} = 0.322$ V s, and the filter is designed to track all three states (e.g., i_d^r , i_q^r and ω_{re}), where 50 particles are used for the particle filter, as a tradeoff between tracking performance in the nominal conditions and CPU execution time and memory requirements. For the particle filter, the variance of the zero-mean Gaussian process noise is set to 0.01 and the variance for zero-mean Gaussian measurement noise is 0.05. The Monte Carlo Markov Chain (MCMC) analysis for particle filtering has been carried out on 10,000 data points, sampled at every $T_s = 0.001$ s.

It is noted that, even though the particle filter does track the states successfully, the residual is not exactly zero. This is because, the parameters provided by the PMSM manufacturer are not necessarily exact and are prone to variations within the tolerance limit.

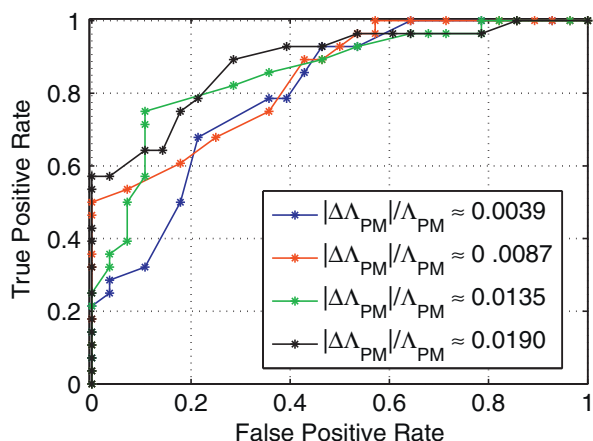


Fig. 10. Receiver operating characteristics (ROC) using particle filtering.

However, more serious is the lack of accurate information on some of the parameters that were experimentally evaluated (e.g., the bearing friction by spin-down test). There is no doubt that a serious fault, which has a noticeable fault signature, would be reflected in the particle filter state estimate error. Such faults are expected to be detected by thresholding techniques. However, in the present case, since the objective is to detect incipient faults as early as possible and having marginal effects on the system performance, the error incurred due to uncertainties in the initial model parameters would mask the fault. In short, a simple thresholding is inadequate.

Instead of using the innovation sequences directly, the histograms of the innovation sequences are obtained, where the innovation is defined as the difference between the measured output and the predicted output. In the nominal condition, the model is a close approximation of the data that are generated, and the system is able to estimate the states with a small error, i.e., the mean and standard deviation of the innovation sequence distribution are small. As the anomaly increases, the model becomes less accurate and the estimation errors become more pronounced. Thus, the histogram of the innovation sequence shows an increase in the variance and the distribution moves away from the nominal distribution. Ultimately, the histograms are expected to converge to a uniform distribution if the filters no longer track the system. The same SVM classifier as before is used with these error histograms as pattern vectors to classify nominal operation from an off-nominal operation. Fig. 10 shows the results of using the particle filter to classify these error patterns. For relatively severe faults, such as 1.90% demagnetization of the PMSM, the fault detection performance of symbolic identification in Fig. 7(a) is modestly better than that of particle filtering in Fig. 10; however, the overall performance of symbolic identification, as seen in all three plots in Fig. 7, significantly exceeds that obtained by using particle filtering. The rationale for superior performance of the symbolic technique is that the nominal model of the PMSM is not assumed and the parameters are not estimated; rather the model is learned from the specific PMSM at hand.

6. Summary, conclusions, and future work

In this paper, some of the critical and practical issues regarding the problem of health monitoring of multi-component human-engineered systems have been discussed, and a syntactic method of fault detection has been proposed. The two primary features of the proposed concept are: (i) *symbolic identification* and (ii) *pseudo-learning*. This paper also reports a novel experimental procedure for achieving controlled accelerated deterioration of magnetic strengths in PMSMs. The theoretical framework has been applied

to data obtained from these demagnetization experiments and has been shown to be able to detect incipient faults with subtle fault signatures in the presence of process and measurement noise.

The reported work is a step toward building a real-time data-driven tool for estimation of parametric conditions in non-linear dynamical systems. Further theoretical, computational, and experimental work is necessary before the symbolic dynamic filtering (SDF)-based fault detection tool can be considered for incorporation into the instrumentation and control system of commercial-scale plants. The following theoretical aspects are currently under investigation:

- Development of a multi-dimensional partitioning for a multi-input multi-output (MIMO) system, which should be computationally inexpensive.
- Estimation of a theoretical bound on the error incurred in this process of fault detection.
- Estimation of a lower bound $|\Sigma|_{min}$ for the alphabet size.
- Investigation of sensitivity of the algorithm on the signal to noise ratio (SNR).
- Fault detection based on statistically non-stationary data collected during transient operations.
- Construction of a multi-class support vector machine for fault detection and fault class identification.
- External validation, where the data generated from one machine is used for training and the data from other different machines for testing, to provide a more accurate estimate of the effectiveness of the underlying algorithms.

Appendix A. List of symbols

Nomenclature

i	stator current (A)
v	voltage (V)
R_s	stator resistance (Ω)
L	inductance (H)
ω	rotor velocity (rad/s)
Ω	steady state rotor velocity (rad/s)
T	torque (N m)
B	bearing friction coefficient (N m s)
J	rotational moment of inertia (kg m^2)
P	number of pole pairs
Λ_{PM}	permanent magnet flux linkage (Vs)
θ	rotor angle (rad)
\mathbf{J}	90° rotation matrix

Superscripts and subscripts

d	direct axis in equivalent 2-phase representation
q	quadrature axis in equivalent 2-phase representation
r	rotor reference frame
e	electrical reference frame
$3ph$	3 phase
a, b, c	three phases in the 3-phase representation
$l-l$	line to line

References

- [1] W. le Roux, R. Harley, T. Habetler, Detecting rotor faults in low power permanent magnet synchronous machines, *IEEE Transactions on Power Electronics* 22 (1) (2007) 322–328.
- [2] P. Broersen, Estimation of parameters of non-linear dynamical systems, *International Journal of Non-linear Mechanics* 9 (1974) 355–361.
- [3] P. Van Lith, H. Witteveen, B. Betlem, B. Roffel, Multiple nonlinear parameter estimation using pi feedback control, *Control Engineering Practice* 9 (2001) 517–531.
- [4] J. Ching, J. Beck, K. PorterChin, Bayesian state and parameter estimation of uncertain dynamical systems, *Probabilistic Engineering Mechanics* 21 (1) (2006) 81–96.

- [5] S. Julier, J. Uhlmann, H. Durrant-Whyte, A new method for the nonlinear transformation of means and covariances in filters and estimators, *IEEE Transactions on Automatic Control* 45 (3) (2000) 477–482.
- [6] C. Bremer, D. Kaplan, Markov chain monte carlo estimation of nonlinear dynamics from time series, *Physica D* 160 (2001) 116–126.
- [7] Y. Wang, L. Geng, Bayesian network based fault section estimation in power systems., in: *IEEE Region 10 Annual International Conference, TENCON*, Hong Kong, China, November, 2006.
- [8] A. Hoffman, N. van der Merwe, The application of neural networks to vibrational diagnostics for multiple fault conditions, *Computer Standards & Interfaces* 24 (2) (2002) 139–149.
- [9] B. David, G. Bastin, Parameter estimation in nonlinear systems with auto and crosscorrelated noise, *Automatica* 38 (2002) 81–90.
- [10] R. Ghanem, F. Romeo, A wavelet-based approach for model and parameter identification of non-linear systems, *International Journal of Non-linear Mechanics* 36 (2001) 835–859.
- [11] L. Yao, W. Sethares, Nonlinear parameter estimation via the genetic algorithm, *IEEE Transactions on Signal Processing* 42 (4) (1994) 927–935.
- [12] J. Ruiz, A. Espinosa, L. Romeral, J. Cusid, Demagnetization diagnosis in permanent magnet synchronous motors under non-stationary speed conditions, *Electric Power Systems Research* 80 (10) (2010) 1277–1285.
- [13] A. Ray, Symbolic dynamic analysis of complex systems for anomaly detection, *Signal Processing* 84 (7) (2004) 1115–1130.
- [14] V. Rajagopalan, A. Ray, Symbolic time series analysis via wavelet-based partitioning, *Signal Processing* 86 (11) (2006) 3309–3320.
- [15] A. Subbu, A. Ray, Space partitioning via Hilbert transform for symbolic time series analysis, *Applied Physics Letters* 92 (08) (2008) 084107.
- [16] Y. Wen, A. Ray, A stopping rule for symbolic dynamic filtering, *Applied Mathematics Letters* 2342 (9) (2010) 1125–1128.
- [17] M.M. Kokar, On consistent symbolic representations of general dynamic systems. *IEEE Transactions on Systems, Man and Cybernetics* 25 (8) (1995) 1231–1242.
- [18] F. Takens, *Detecting Strange Attractors in Turbulence.*, Springer, Berlin/Heidelberg, Germany, 1981, 898/1981.
- [19] J. Beirlant, E.J. Dudewicz, L. Gyrfi, E.C. Meulen, Nonparametric entropy estimation: an overview, *International Journal of the Mathematical Statistics Sciences* 6 (1997) 17–39.
- [20] S. Chakraborty, S. Sarkar, A. Ray, Symbolic identification for fault detection in aircraft gas turbine engines, *Proceedings of the Institution of Mechanical Engineers, Part G: Journal of Aerospace Engineering*, 2012, Available: <http://pig.sagepub.com/content/early/2011/11/06/0954410011409980.abstract> (Online).
- [21] K.S. Narendra, M.A.L. Thathachar, *Learning Automata: An Introduction.*, Prentice-Hall, Englewood Cliffs, NJ, USA, 1989.
- [22] C.M. Bishop, *Pattern Recognition and Machine Learning.*, Springer, New York, NY, USA, 2006.
- [23] W. Thomson, M. Fenger, Current signature analysis to detect induction motor faults., *Industry Applications Magazine, IEEE* 7 (July/August (4)) (2001) 26–34.
- [24] J. Rosero, L. Romeral, J. Ortega, J. Urresty, Demagnetization fault detection by means of hilbert huang transform of the stator current decomposition in pmsm, in: *IEEE International Symposium on Industrial Electronics, ISIE 2008*, 30 2008–July 2 2008, pp. 172–177.
- [25] M. Benbouzid, A review of induction motors signature analysis as a medium for faults detection, *IEEE Transactions on Industrial Electronics* 47 (5) (2000) 984–993.
- [26] M. Arulampalam, S. Maskell, N. Gordon, T. Clapp, A tutorial on particle filters for online nonlinear/non-Gaussian Bayesian tracking, *IEEE Transactions on Signal Processing* 50 (2) (2002) 174–188.